Journal of Power Sources 183 (2008) 512–517

Contents lists available at ScienceDirect

Journal of Power Sources

journal homepage: www.elsevier.com/locate/jpowsour

Use of $La_{0.75}Sr_{0.25}Cr_{0.5}Mn_{0.5}O_3$ materials in composite anodes for direct ethanol solid oxide fuel cells

Xiao-Feng Ye, S.R. Wang*, Z.R. Wang, Q. Hu, X.F. Sun, T.L. Wen, Z.Y. Wen

Shanghai Institute of Ceramics, Chinese Academy of Sciences (SICCAS), 1295 Dingxi Road, Shanghai 200050, PR China

ARTICLE INFO

Article history:
Received 12 April 2008
Received in revised form 15 May 2008
Accepted 20 May 2008
Available online 9 July 2008

Keywords:
Solid oxide fuel cell
Perovskite
Mixed conductors
Composite anode
Carbon deposition

ABSTRACT

The perovskite system $La_{1-x}Sr_xCr_{1-y}M_yO_{3-\delta}$ (M, Mn, Fe and V) has recently attracted much attention as a candidate material for the fabrication of solid oxide fuel cells (SOFCs) due to its stability in both H_2 and CH_4 atmospheres at temperatures up to 1000 °C. In this paper, we report the synthesis of $La_{0.75}Sr_{0.25}Cr_{0.5}Mn_{0.5}O_3$ (LSCM) by solid-state reaction and its employment as an alternative anode material for anode-supported SOFCs. Because LSCM shows a greatly decreased electronic conductivity in a reducing atmosphere compared to that in air, we have fabricated Cu-LSCM-ScSZ (scandia-stabilized zirconia) composite anodes by tape-casting and a wet-impregnation method. Additionally, a composite structure (support anode, functional anode and electrolyte) structure with a layer of Cu-LSCM-YSZ (yttria-stabilized zirconia) on the supported anode surface has been manufactured by tape-casting and screen-printing. Single cells with these two kinds of anodes have been fabricated, and their performance characteristics using hydrogen and ethanol have been measured. In the operation period, no obvious carbon deposition was observed when these cells were operated on ethanol. These results demonstrate the stability of LSCM in an ethanol atmosphere and its potential utilization in anode-supported SOFCs.

1. Introduction

Solid oxide fuel cell (SOFC), which converts the chemical energy of gaseous fuels to electricity through electrochemical processes, is considered as a promising clean power source for a variety of stationary and mobile applications [1,2]. An obvious advantage of SOFCs over other types of fuel cells is that they can directly use hydrocarbon fuels without external reforming. Because ethanol is regarded as a renewable and green fuel [3], the efforts of our group have been directed towards the development of SOFCs fed with ethanol as a fuel. The anode materials of SOFCs should meet several basic requirements such as high electronic conductivity, excellent catalytic properties for fuel oxidation reactions, chemical stability and thermal compatibility with other cell components and sufficient porosity in a high-temperature reducing environment [4].

Although the commonly used Ni/YSZ cermet anodes show high electrochemical activity in H_2 oxidation and long-term stability under SOFC operating conditions, they give rise to carbon deposition and display rapid performance degradation while using hydrocarbon fuels [2,5]. Therefore, in recent years, much effort has been directed towards the development of Ni-free oxides as SOFC anode materials such as ceria [6,7], titanate and lanthanum chromite-based oxides [8–10]. Among them, the perovskite system $La_{1-x}Sr_xCr_{1-y}M_yO_3$ (M, Mn, Fe and V) has recently attracted much attention due to its stability in both H_2 and CH_4 atmospheres at temperatures up to 1000 °C. $LaCrO_3$-based oxides display a low tendency for carbon formation, and Ca and Sr substitution at the A-site, or Mn, Fe and Ni substitution at the B-site improve the catalytic activity for methane conversion [11]. Recently, Tao and Irvine [12] reported that $La_{0.75}Sr_{0.25}Cr_{0.5}Mn_{0.5}O_3$ (LSCM) achieved a level of performance comparable to that of Ni/YSZ in both hydrogen and methane. However, due to the low electronic conductivity of LSCM in reducing atmospheres, the ensuing researches have been focused on electrolyte-supported single cells [13–15] and cathode-supported single cells [16,17].

In this paper, we describe the synthesis of $La_{0.75}Sr_{0.25}Cr_{0.5}Mn_{0.5}O_3$ by solid-state reaction methods and its employment in fabrication of two anode-supported single cells by different techniques. The first cell, with a Cu-LSCM-ScSZ anode, was fabricated by tape-casting and a wet-impregnation method. Within the anode of this cell, the ionic conducting phase ScSZ increases the number of reaction sites, while the impregnated copper increases electronic conductivity of the anode. The second cell has a Cu-LSCM-YSZ layer screen-printed on the supported anode, which is one of the three layers (anode support layer, anode functional layer, and electrolyte) of the composite membrane typically used by our group. The power densities of this cell reached 584 and 384 mW cm^{-2} at

* Corresponding author. Tel.: +86 21 52411520; fax: +86 21 52413903.
E-mail addresses: yexf@mail.sic.ac.cn (X.-F. Ye), srwang@mail.sic.ac.cn (S.R. Wang).

0378-7753/$ – see front matter © 2008 Elsevier B.V. All rights reserved.
doi:10.1016/j.jpowsour.2008.05.064

800 °C in hydrogen and ethanol steam, respectively. In particular, this anode structure showed very good stability over a discharging period of 120 h in ethanol atmosphere, with stable power density of 300 mW cm^{-2}. All of these results indicate the potential utility of $La_{0.75}Sr_{0.25}Cr_{0.5}Mn_{0.5}O_3$ in anode-supported SOFCs running on hydrocarbon fuels.

2. Experimental

2.1. Sample preparation and characterization

The anode material $La_{0.75}Sr_{0.25}Cr_{0.5}Mn_{0.5}O_3$ was synthesized from La_2O_3 (98.4%), $SrCO_3$ (99.8%), Cr_2O_3 (98.5%) and $MnCO_3$ (93.9%) by solid-state reaction. All of these oxides and carbonates used in the synthesis were supplied by Shanghai Chem. Ltd., China. The powders were mixed in stoichiometric proportions and ball-milled with de-ionized water for 3 h. The dried mixture was then pre-heated at 1000 °C for 5 h to decompose the carbonate, and then the powders were pressed into pellets and sintered at 1450 °C for 15 h in air. After smashing, ball-milling, and sifting, LSCM powder was finally obtained.

Portions of LSCM and ScSZ (99.99% pure; Daiichi Kigenso, Japan) powders were mixed, co-fired in air at 1450 °C for 3 h, and then characterized by XRD analysis to ensure their chemical compatibility. The phases of LSCM and ScSZ powders were identified by means of a Rigaku XRD diffractometer at room temperature, using monochromatic Cu Kα radiation. To measure the thermal expansion coefficients (TECs) of LSCM and SSZ, the respective powders were pressed into cylinder samples with a diameter of 5 mm and a length of 16 mm, respectively. After sintering at 1450 °C for 3 h, the TECs of these samples were measured by means of a NETZSCH DIL 402PC dilatometer. The measurement was carried out over the temperature range from 20 to 1300 °C at heating rate of 5 K min^{-1}.

2.2. Preparation of Cu-$La_{0.75}Sr_{0.25}Cr_{0.5}Mn_{0.5}O_3$-ScSZ composite anodes

Porous LSCM-ScSZ matrix was prepared by tape-casting of a slurry containing LSCM, ScSZ and 10 wt% ammonium oxalate (99.8% pure, Shanghai Chem. Ltd., China.) as a pore former. The solvent system used in this paper was the azeotropic mixture of butanone and ethanol. Triethanolamine, poly-vinyl-butyral (PVB) and a mixture of polyethylene glycol (PEG 200) and dibutyl-*o*-phthalate (DOP) were used as dispersant, binder, and plasticizer, respectively. The green tapes were subsequently sintered at 1450 °C for 3 h. The LSCM-ScSZ/ScSZ dual-layer membrane was fabricated by two-fold tape-casting and co-sintering processes.

The obtained porous LSCM-ScSZ matrix was impregnated with an aqueous solution of $Cu(NO_3)_2{\cdot}3H_2O$ and then calcinated at 450 °C to form oxides. After typically five successive impregnation steps, the final composition of the anode used in this work was 10 wt%Cu/45 wt%LSCM/45 wt%ScSZ, which was calculated by the weight change of the porous LSCM-ScSZ matrix before and after the wet-impregnation treatment.

2.3. Preparation of a three-layer anode structure

The anode-supported electrolyte membrane composed of NiO-YSZ supported anode layer and NiO-ScSZ anode functional layer and ScSZ electrolyte was fabricated by multi-layer tape-casting and co-sintering, as has been typically employed by our group. Details of its manufacture can be found elsewhere [18].

Copper oxides, LSCM, and 8YSZ (Tosoh Co.) powders in the mass ratio of 3:3.5:3.5 were mixed in a planetary mill with ethanol as solvent for 1 h to ensure random distribution of each phase. The dried mixture was ground with terpineol-based slurry in anagate mortar to prepare a paste, which was then screen-printed onto the Ni-YSZ-supported anode surface and sintered at 1100 °C for 3 h to form the surface anode layer.

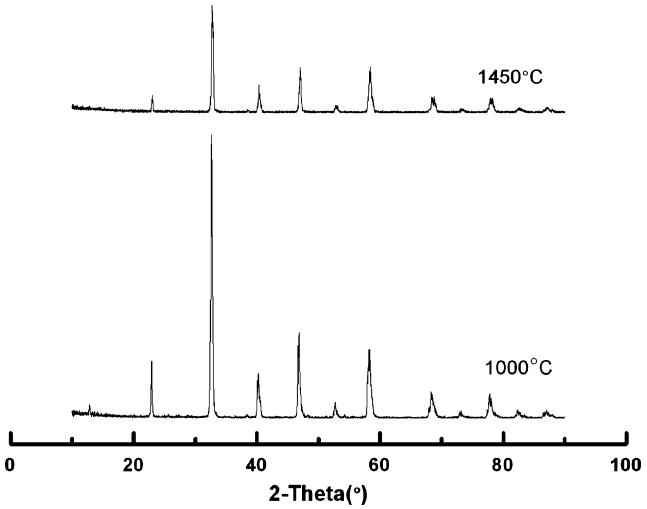

Fig. 1. XRD patterns of $La_{0.75}Sr_{0.25}Cr_{0.5}Mn_{0.5}O_3$ (LSCM) powders pre-heated at 1000 °C for 5 h and sintered at 1450 °C for 15 h, respectively.

2.4. Cell fabrication and testing

The cathode material used in this work was $(Pr_{0.7}Ca_{0.3})_{0.9}MnO_3$ (PCM), which was provided by co-workers from our group. A PCM cathode, of area 1.33 cm^2, was screen-printed onto a section of the ScSZ electrolyte surface of diameter 25 mm, which was cut from the composite membrane mentioned in sections 2.2 and 2.3. The cathode was sintered in air at 1200 °C for 3 h. The microstructure and morphology of the cell structure were examined by scanning electron microscopy (SEM, JXA-8100, JEOL Co. Ltd., Japan).

SOFC tests were carried out in a single cell test set-up, which has been illustrated in our previous publications [19,20]. A glass ring was attached to the electrolyte side of the cell to prevent the oxygen leakage. Pt meshes and Au lead wires as the current collector were attached to the electrode surface using a Pt paste, and a four-probe configuration was adopted in the electrochemistry tests. All the anodes were evaluated by the same testing procedure. The anodes were fully reduced in an H_2 atmosphere at 800 °C for several hours prior to cell testing, and then the requisite measurements were made at temperatures of 750, 800 and 850 °C.

Hydrogen or gasified ethanol/water mixture (with volume ratio 2:1) was used as the fuel and oxygen was used as the oxidant. The fuel and oxidant flow rates were both set at 25 mL min^{-1}, and the liquid fuel was vaporized in a water bath (70 °C) and then passed over the anode surface by a flow of nitrogen. The current–voltage curves and electrochemical impedance spectra (EIS) were obtained using an Electrochemical Workstation (IM6e, ZAHNER). The impedance spectra of the cells were recorded at open circuit voltage (OCV) over the frequency range from 100 mHz to 8 mHz with an excitation potential of 20 mV.

3. Results and discussion

3.1. LSCM characterization

3.1.1. The phase and stability

Fig. 1 shows the X-ray diffraction (XRD) patterns of LSCM powder pre-heated at 1000 °C and sintered at 1450 °C, which

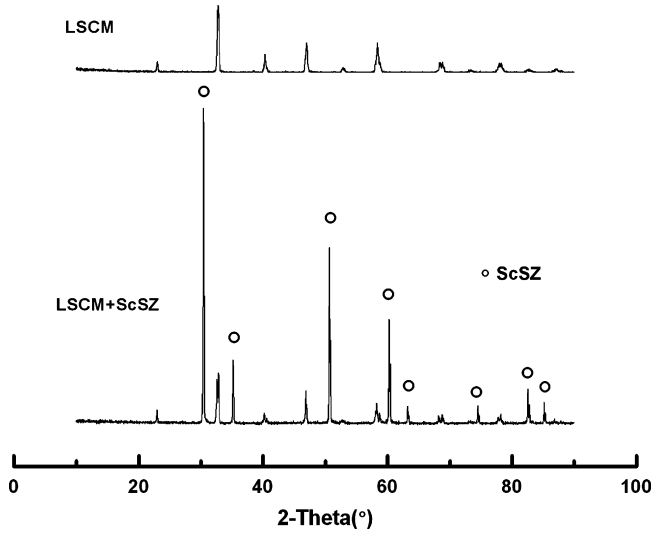

Fig. 2. XRD patterns of $La_{0.75}Sr_{0.25}Cr_{0.5}Mn_{0.5}O_3$ (LSCM) powder sintered at 1450 °C and of an LSCM-ScSZ mixture (1:1, w/w) co-fired at 1450 °C.

indicated the formation of the perovskite phase of the $La_{0.75}Sr_{0.25}Cr_{0.5}Mn_{0.5}O_3$ powder. Room temperature XRD patterns of LSCM and co-fired LSCM-ScSZ powders are shown in Fig. 2, in which no apparent new phase was observed. This also proves the chemical compatibility of LSCM with ScSZ up to at least 1450 °C.

3.1.2. Thermal expansion behavior

The thermal expansion behaviors of LSCM, LSCM-ScSZ, and ScSZ are shown in Fig. 3. The average linear thermal expansion coefficient (TEC) of LSCM in the temperature range of 25–900 °C is $11.8 \times 10^{-6}\,K^{-1}$, which is somewhat higher than the $11.4 \times 10^{-6}\,K^{-1}$ reported by Jiang et al. [21] and the $9.3 \times 10^{-6}\,K^{-1}$ reported by Tao and Irvine [12] for the same materials. Furthermore, the average TEC of LSCM-ScSZ and ScSZ between 25 and 900 °C are $11.5 \times 10^{-6}\,K^{-1}$ and $10.6 \times 10^{-6}\,K^{-1}$, respectively. TEC matching of the two phases was achieved, which makes it possible to fabricate an LSCM-ScSZ/ScSZ structure by tape-casting and co-sintering. The large area anode-supported electrolyte film is very important for the manufacture of planar SOFCS with potential for practical utilization.

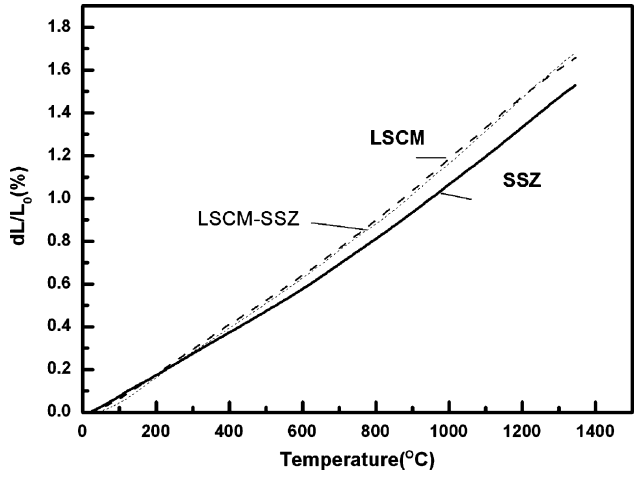

Fig. 3. Thermal expansion of LSCM, LSCM-ScSZ, and ScSZ at high temperatures in air.

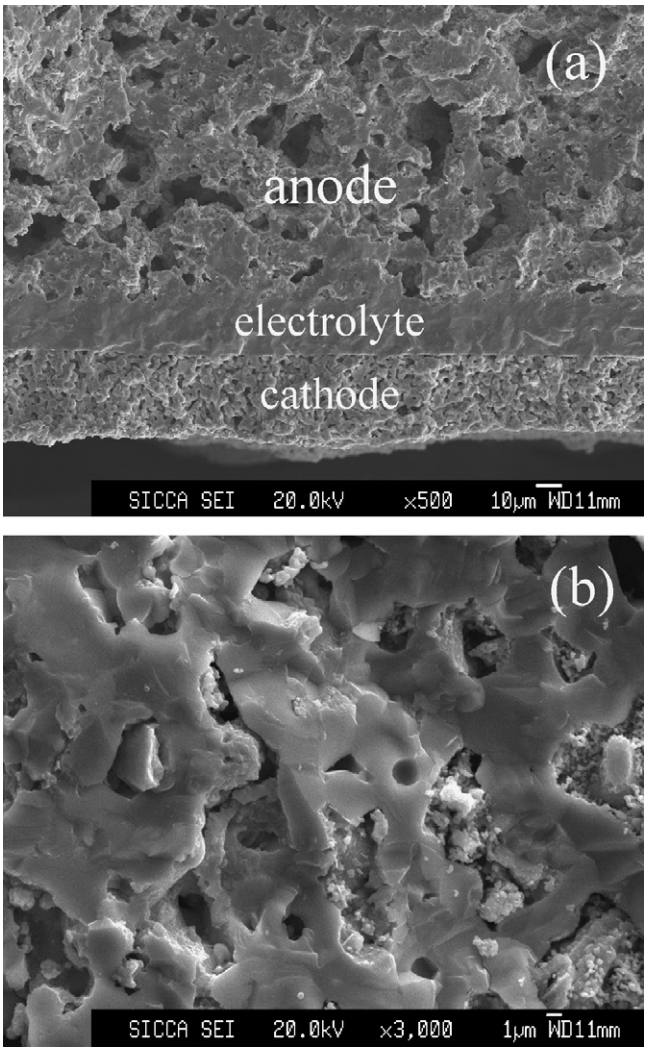

Fig. 4. SEM images of a Cu-LSCM-ScSZ/ScSZ/PCM single cell showing three layers (a) and the anode matrix after operation in ethanol (b).

3.2. Cu-LSCM-ScSZ/ScSZ/PCM single cell

3.2.1. SEM characterization

Fig. 4. shows the cross-sectional SEM images of the Cu-LSCM-ScSZ/ScSZ/PCM single cell (a) and the anode matrix after operation (b). As can be seen in Fig. 4(a), both a porous anode and a dense electrolyte were obtained by tape-casting and co-sintering process, and the two layers have good contact without obvious segregation seen at the interface. A tight junction can also be seen at the interface between the electrolyte and the cathode layer. The three layers (anode, electrolyte and cathode) have thicknesses of about 600, 20, and 30 μm, respectively. Meanwhile, it can be seen in Fig. 4(b) that copper particles had been homogeneously impregnated into the LSCM-ScSZ matrix, without deposition of carbon in the anode. However, the LSCM obtained by solid-state reaction showed coarse particle size and sintered with ScSZ particles. The catalytic activity of the LSCM towards ethanol conversion was thus retarded and the length of three-phase boundary (TPB) was decreased.

3.2.2. Single cell performance

Fig. 5 presents the curves of voltage and power density vs. current density for a single cell with a Cu-LSCM-ScSZ anode while running on humidified hydrogen and ethanol stream. It can be

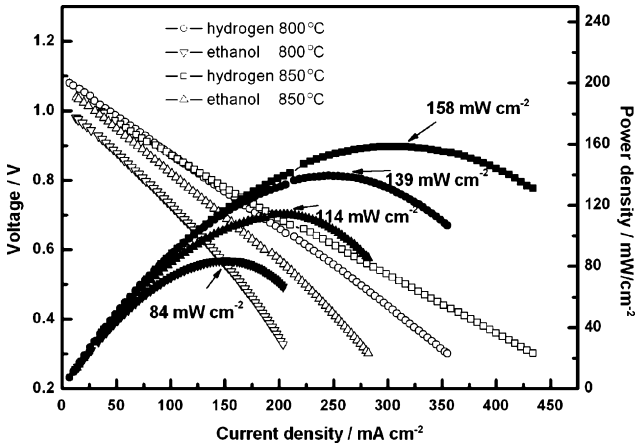

Fig. 5. Voltage (open) and power density (closed) vs. current density for the Cu-LSCM-ScSZ/ScSZ/PCM single cell in hydrogen and ethanol steam at 800 and 850 °C, respectively.

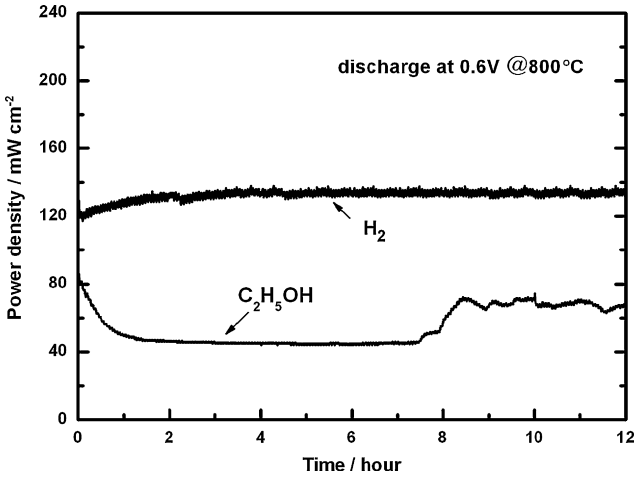

Fig. 7. Power density at 0.6 V as a function of time for the Cu-LSCM-ScSZ/ScSZ/PCM single cell in hydrogen and ethanol steam at 800 °C.

seen in Fig. 5 that the maximum power densities in hydrogen and ethanol steam reached 139 and 84 mW cm^{-2} at 800 °C respectively, while the corresponding values at 850 °C were 158 and 114 mW cm^{-2}. The open circuit voltage (OCV) of the cell in hydrogen and ethanol reached approximately 1.1 and 1.05 V, which proves that the ScSZ electrolyte was tightly sintered at 1450 °C. However, the cell performance was lower than that obtained with the electrolyte-supported single cell employing a Cu-LSCM anode [13]. From the impedance spectra in Fig. 6, we can see that the cell performance was greatly inhibited by the high ohmic resistance, which may be estimated as about 300 mΩ cm^2 at 800 °C from the real-axis intercept at high frequency. A higher copper loading is probably required to improve the anode conductivity. The polarization resistance of the cell was found to be approximately 1.8 and 2.5 Ω cm^2 in hydrogen and ethanol atmospheres, respectively. In the impedance spectra of the cell, we found that when the fuel was changed, the high-frequency arc almost remained almost unchanged, while the low-frequency arc increased significantly. The low-frequency arc is probably related to the anode polarization and thus accounts for a major part of the total polarization resistance. Thus, the porosity of the anode and the particle size of LSCM might be optimized to increase the anode performance.

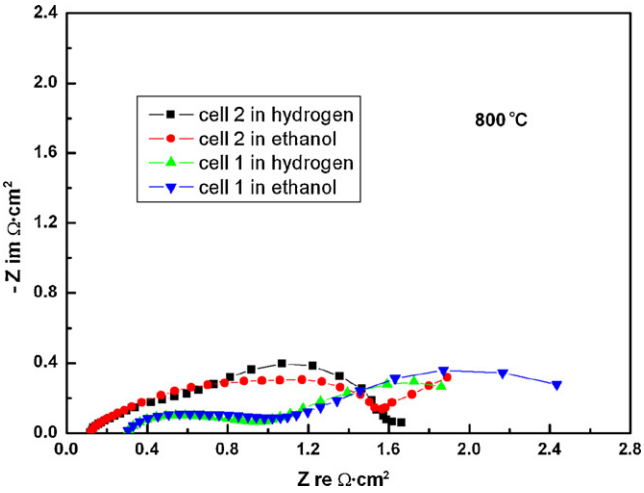

Fig. 6. Impedance spectra for cell 1 (Cu-LSCM-ScSZ/ScSZ/PCM) and cell 2 (Cu-LSCM-YSZ/Ni-YSZ/Ni- ScSZ/ScSZ/PCM) while running on hydrogen and ethanol steam at 800 °C.

As shown in Fig. 7, the stability of the Cu-LSCM-ScSZ composite anode in hydrogen and ethanol steam was evaluated by discharging it at 0.6 V over a period of 12 h. Considering the thermal stability of copper, the operating temperature was set at 800 °C. With hydrogen, the power density increased from 120 to about 135 mW cm^{-2} during the first 4 h of electrode activation, and in the remaining 8 h the cell performance was rather stable. In the process of electrode activation, the fuel gradually covers the surface of the reaction sites, and it has also been reported that the conductivity of the LSCM material increases with increasing oxygen pressure, which was generated owing to the production of water in the anode [12,15]. In case of the ethanol fuel, the activation process was extended to 8 h, which is probably due to the greater mass and slower gas-phase diffusion of ethanol molecules. After the cell had been fully activated, a stable power density of around 75 mW cm^{-2} was achieved. No carbon formation was seen on the anode surface after experiments, which was further verified by the SEM images in Fig. 4(b). As discussed above, the Cu-LSCM-ScSZ anode showed its good stability, even though its performance was poor.

3.3. Cu-LSCM-YSZ/Ni-YSZ/Ni-ScSZ/ScSZ/PCM single cell

3.3.1. SEM characterization

SEM photographs of a Cu-LSCM-YSZ/Ni-YSZ/Ni- ScSZ/ScSZ/PCM single cell are shown in Fig. 8. The cell shown in Fig. 8(a) consisted of five layers, (1) a porous PCM cathode, (2) a dense ScSZ electrolyte, (3) a Ni-ScSZ anode functional layer, (4) a porous Ni/YSZ-supported anode and (5) a porous Cu-LSCM-YSZ surface anode layer. The thicknesses of these layers are about 20, 20, 20, 500, and 20 μm, respectively. The supported anode has high porosity but not a very uniform pore size, and the surface anode layer shows a good microstructure. As illustrated in Fig. 8(b), the layers are in good contact with each other; in particular, the supported anode layer adheres well to the surface anode layer.

3.3.2. Single cell performance

Fig. 9 presents the curves of voltage and power density vs. current density of a single cell with a Cu-LSCM-YSZ anode surface layer, which was fed with humidified hydrogen and ethanol stream at 800 and 750 °C. From Fig. 9, it can be seen that the maximum power densities in hydrogen and ethanol steam were 534 and 384 mW cm^{-2}, respectively, at 800 °C, while the corresponding values were 366 and 231 mW cm^{-2} at 750 °C. The cell performance is improved markedly than that of the first single cell mentioned above, and

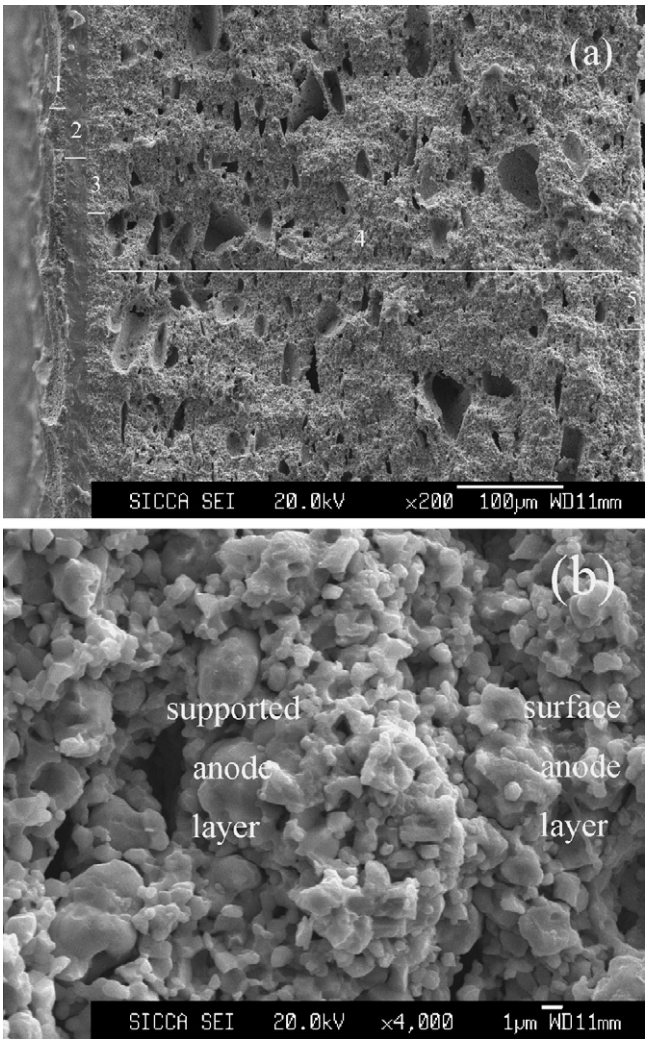

Fig. 8. SEM photographs of the Cu-LSCM-YSZ/Ni-YSZ/Ni-ScSZ/ScSZ/PCM single cell containing five layers (a) and the interface between the surface anode layer and the supported anode layer after 140 h of operation (b).

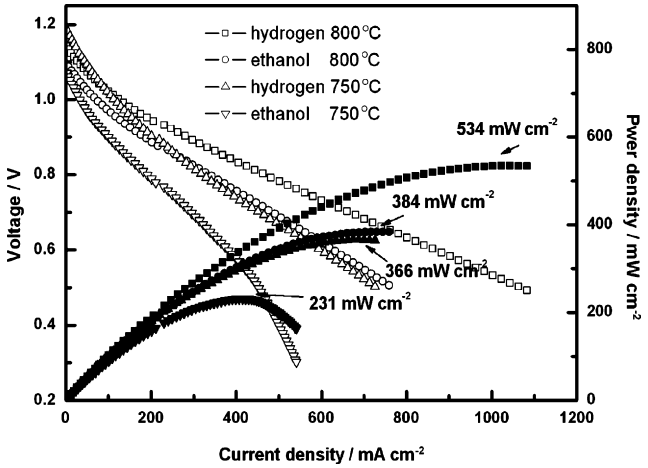

Fig. 9. Voltage (open) and power density (closed) vs. current density for the Cu-LSCM-YSZ/Ni-YSZ/Ni-ScSZ/ScSZ/PCM single cell in hydrogen and ethanol steam at 750 and 800 °C.

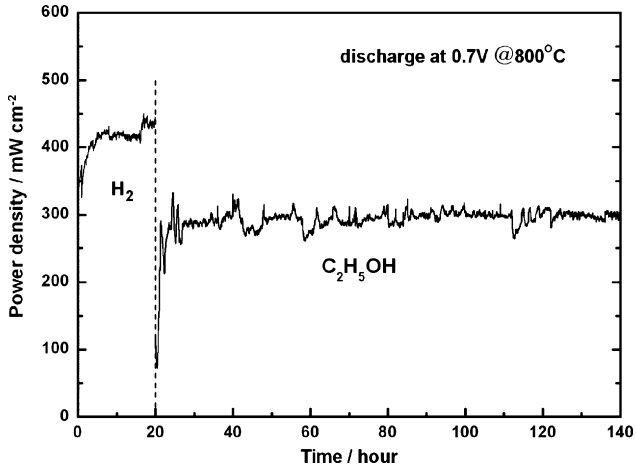

Fig. 10. Power density at 0.7 V as a function of time for the Cu-LSCM-YSZ/Ni-YSZ/Ni-ScSZ/ScSZ/PCM single cell in hydrogen and ethanol steam at 800 °C.

while discharging at 700 mA cm^{-2}, the utilization factor for H_2 and O_2 is about 26 and 13% by calculation, respectively. As seen in Fig. 6, the ohmic resistance of 120 mΩ cm^2 is much lower than that of the first single cell, not only because of the higher copper loading in the Cu-LSCM-YSZ layer, but also because the surface layer is so thin that the Ni-YSZ anode is to a large extent responsible for the overall conductivity of the anode. In contrast to the previous spectrum, the impedance spectrum is composed of three arcs. Moreover, we also found that when the fuel was changed, the first and second arcs almost remained almost unchanged, while the low-frequency arc increased significantly. Because more layers are sintered within this cell, especially the three layers that constitute the anode, the gas diffusion processes for ethanol and the possible steam reforming product are assumed to be more hampered.

The discharge characteristics at 0.7 V in hydrogen and ethanol steam at 800 °C are presented in Fig. 10. While operating on hydrogen, the cell performance initially improved gradually from 350 to 440 mW cm^{-2}. When the single cell performed in an almost stable manner, the fuel was switched to ethanol steam. After an anode activation process of about 4 h, the single cell performance kept constant at around 300 mW cm^{-2} without any degradation over a period of 120 h. Although the tendency for carbon deposition increased with distance from the electrolyte, the high catalytic of Cu-LSCM-YSZ over ethanol conversion might inhibit ethanol pyrolysis. Therefore, the anode structure can reach a stable performance output in ethanol fuel in spite of the presence of nickel. It is still not clear whether the ethanol fuel is first internally reformed or is oxidized directly. In future work, we will employ mass spectroscopy and gas chromatography to measure the concentration of ethanol in the fuel stream and the composition of the anode exhaust gas in order to analyze the reaction mechanism.

During the period of operation, the impedance spectra of this cell at open circuit voltage were also recorded at time intervals of 40 h to get more information of this anode structure; these spectra are shown in Fig. 11. It may be noted that ohmic resistance remained unchanged over the whole time, indicating interface stability of the anode structure. Meanwhile, the polarization resistance gradually decreased with operation time probably due to sufficient diffusion and ethanol conversion at the TPBs. These results also indicated the stability of the anode structure, since the polarization resistance increased when the carbon deposition happened in the anode [22]. After 120 h of operation, the Cu-LSCM-YSZ surface layer and the supported anode were still very well connected. Neither delamination nor leakage was discerned in Fig. 8(b). Fur-

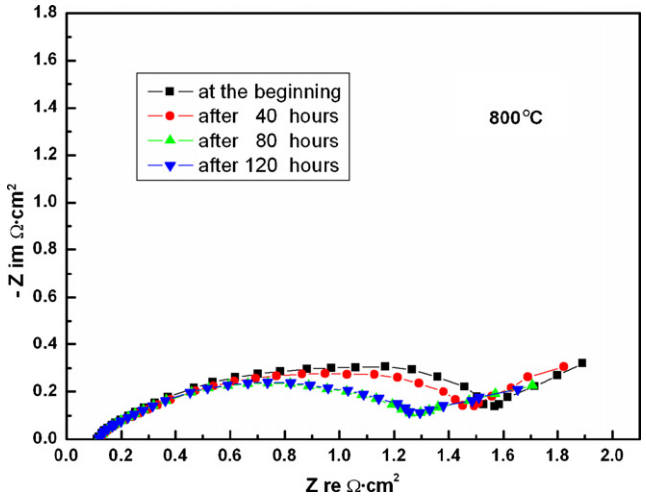

Fig. 11. Impedance spectra for the Cu-LSCM-YSZ/Ni-YSZ/Ni-ScSZ/ScSZ/PCM single cell as a function of operation time running on ethanol steam at 800 °C.

thermore, there was no carbon formation seen in the anode matrix.

4. Conclusions

We have synthesized $La_{0.75}Sr_{0.25}Cr_{0.5}Mn_{0.5}O_3$ by solid-state reaction methods and have employed it in the fabrication of two anode-supported SOFCs by different techniques. The first cell with a Cu-LSCM-ScSZ anode was fabricated by wet tape-casting and a wet-impregnation method. Within the anode of this cell, the ionic conducting phase ScSZ increases the number of reaction sites, and the impregnated copper increases the electronic conductivity of the anode. Due to the low conductivity of LSCM in a reducing atmosphere and its coarse particle size, this first cell behaved poorly albeit with good stability in both hydrogen and ethanol atmospheres. The second cell has a Cu-LSCM-YSZ layer screen-printed on the surface of the supported anode, which is one of the three layers (anode support layer, anode functional layer and electrolyte) of the composite membrane typically used by our group. The power densities of this cell reached 584 and 384 mW cm^{-2} at 800 °C in hydrogen and ethanol steam, respectively. In particular, this anode structure showed very good stability over a discharging period of 120 h in ethanol atmosphere with a stable power density of 300 mW cm^{-2}. Thus, it may be supposed that a Cu-LSCM-YSZ composite anode surface layer is effective in suppressing carbon deposition. From the point of view of the performance and manufacturing costs, the second cell is suggestive of a more promising technique. All of these results indicate the potential utilization of $La_{0.75}Sr_{0.25}Cr_{0.5}Mn_{0.5}O_3$ materials in anode-supported structures of SOFCs fed with ethanol fuels, and that the cell performance may be improved if LSCM powders with fine particle size are applied.

Acknowledgements

The authors would like to express their appreciation for financial support from the Chinese Government High Tech Developing Project (2003AA517010), and also thank Mr. Xiong for providing PCM powders.

References

[1] S. McIntosh, R.J. Gorte, Chem. Rev. 104 (2004) 4845–4865.
[2] S.P. Jiang, S.H. Chan, Mater. Sci. Technol. 20 (2004) 1109–1118.
[3] K. Sasaki, K. Watanabe, Y. Teraoka, J. Electrochem. Soc. 151 (2004) A965–A970.
[4] N.Q. Minh, J. Amer. Ceram. Soc. 76 (1993) 563.
[5] S.P. Jiang, S.H. Chan, J. Mater. Sci. 39 (2004) 4405–4439.
[6] S. Park, J.M. Vohs, R.J. Gorte, Nature (London) 404 (2000) 265.
[7] R.J. Gorte, S. Park, J.M. Vohs, C. Wang, Adv. Mater. 12 (2000) 1465.
[8] S. Primdahl, J.R. Hansen, L. Grahl-Madsen, P.H. Larsen, J. Electrochem. Soc. 148 (2001) A74.
[9] P. Holtappels, J. Bradley, J.T.S. Irvine, A. Kaiser, M. Mogensen, J. Electrochem. Soc. 148 (2001) A923.
[10] G. Pudmich, B.A. Boukamp, M. Gonzalez-Cuenca, W. Jungen, W. Zipprich, F. Tietz, Solid State Ionics 135 (2000) 433.
[11] J. Sfeir, P.A. Buffat, P. Mockli, N. Xanthopoulos, R. Vasquez, H.J. Mathieu, J. Van Herle, K.R. Thampi, J. Catal. 202 (2001) 229–244.
[12] S. Tao, J.T.S. Irvine, J. Electrochem. Soc. 151 (2004) A252–A259.
[13] J. Wan, J.H. Zhu, J.B. Goodenough, Solid State Ionics 177 (2006) 1211–1217.
[14] X.C. Lu, J.H. Zhu, Solid State Ionics 178 (2007) 1467–1475.
[15] X.J. Chen, Q.J. Liu, K.A. Khor, S.H. Chan, J. Power Sources 165 (2007) 34–40.
[16] S.P. Jiang, L. Zhang, Y. Zhang, J. Mater. Chem. 17 (2007) 2627–2635.
[17] X.J. Chen, Q.J. Liu, S.H. Chan, N.P. Brandon, K.A. Khor, Electrochem. Commun. 9 (2007) 767–772.
[18] Z. Wang, J. Qian, J. Cao, S. Wang, T. Wen, J. Alloys Compd. 437 (2007) 264–268.
[19] Ye. Xiao-Feng, S.R. Bo Huang, Z.R. Wang, L. Wang, T.L. Xiong, Wen, J. Power Sources 164 (2007) 203–209.
[20] S.R. Xiao-Feng Ye, Z.R. Wang, L. Wang, X.F. Xiong, T.L. Sun, Wen, J. Power Sources 177 (2008) 419–425.
[21] S.P. Jiang, X.J. Chen, S.H. Chan, J.T. Kwok, K.A. Khor, Solid State Ionics 177 (2006) 149157.
[22] J.-H. Koh, Y.-S. Yoo, J.-W. Park, H.C. Lim, Solid State Ionics 149 (2002) 157–166.